Hindawi
Journal of Nanomaterials
Volume 2020, Article ID 8040517, 16 pages
https://doi.org/10.1155/2020/8040517

Research Article

Properties of 3D Printable Poly(lactic acid)/Poly(butylene adipate-co-terephthalate) Blends and Nano Talc Composites

Wattanachai Prasong[1], **Paritat Muanchan**[1], **Akira Ishigami**[1], **Supaphorn Thumsorn**[2], **Takashi Kurose**[2] and **Hiroshi Ito**[1,2]

[1]*Graduate School of Organic Materials Science, Yamagata University, 4-3-16 Jonan, Yonezawa, Yamagata 992-8510, Japan*
[2]*Research Center for GREEN Materials and Advanced Processing (GMAP), 4-3-16 Jonan, Yonezawa, Yamagata 992-8510, Japan*

Correspondence should be addressed to Supaphorn Thumsorn; thumsorn@yz.yamagata-u.ac.jp
and Hiroshi Ito; ihiroshi@yz.yamagata-u.ac.jp

Received 25 December 2019; Revised 23 February 2020; Accepted 28 February 2020; Published 28 March 2020

Guest Editor: Ana C. S. Alcântara

Biodegradable poly(lactic acid) (PLA) filaments have been widely used in the fused deposition modeling (FDM) 3D printing technology. However, PLA has low toughness and low thermal resistance that affects printability and restricts its industrial applications. In this study, PLA was compounded with 0 to 40 wt% of poly(butylene adipate-co-terephthalate) (PBAT) and varied content of nano talc at 0 to 40 wt% in a twin screw extruder. The compounds were reextruded to filaments using a capillary rheometer. PLA/PBAT blends and their composite filaments were printed with a FDM 3D printing machine. Morphology, rheological behaviour, thermal characteristic, surface roughness, and mechanical property of 3D printing of the blends and the composites were investigated. Complex viscosity of the blends and the composites increased with increase of the PBAT and the nano talc contents. The incorporation of the nano talc enhanced crystallization temperature and reduced the coefficient of volume expansion of the composites. It was found that the PLA/PBAT blends and composites were excellent in both printability and dimension stability at PBAT content 10-30 wt% and nano talc up to 10 wt%. Interestingly, it was possible to print the composite filaments at an angle up to 75° during the overhang test without a supporter. From the vertical specimens, the surface roughness improved due to the incorporation of the nano talc. Tensile strength of the blends and the composites decreased, whereas elongation at break increased when the PBAT and the nano talc contents were increased. The reduction of tensile strength was attributed to agglomeration of the PBAT dispersed phase and less adhesion between the nano talc and the matrix. It can be noted that the composite 3D printing product showed superior elongation at break up to 410% by adding nano talc 1 wt%. This result suggests that the ductile 3D printable PLA/PBAT blend and the PLA/PBAT-nano talc composite products can be prepared, which shows potential for the commercialized scale.

1. Introduction

3D printing technology has been popular for rapid prototyping technology, which is flexible design by computer-aided design software without molds [1–9]. Up to date, the development in 3D printing technology in various applications is further required such as small parts or pseudo organs in the medical industry, new fashion clothes in the textile industry, and automotive and construction parts [2–4, 10, 11]. There are various types of 3D printing technology, which are available according to purpose and material selections. Fused deposition modeling (FDM) is widely used for polymer materials in the 3D printing technology [1–14]. Structural fabricated in FDM 3D printing is operated by extruding molten thermoplastic filament layer-by-layer deposition [5–9, 12–16]. Nevertheless, the drawbacks of 3D printing technology deal with low mechanical properties, long processing time, conflicting mass-production scale, poor dimensional stability due to thermal-induced volume shrinkage, and heat distortion of materials [2, 3]. Thus, development of 3D printing machines, software programs, 3D printable materials, and so on is still open in the FDM 3D printing technology.

The most popular thermoplastic filaments in 3D printing technology are poly(lactic acid) (PLA) and acrylonitrile-butadiene-styrene (ABS), which were derived from bio-based and petroleum-based resources, respectively [3, 4]. Owing to the global environmental problems, biodegradable and compostable plastics are becoming the key materials for the sustainable development in our future society. Therefore, material development and optimizing processability of biodegradable plastics in 3D printing, especially PLA, have been promising for various industrial fields [2–6, 12–15]. Nevertheless, PLA is known for its brittleness, low elongation at break, low impact strength, slow crystallization, and low heat distortion temperature. The incorporation of polymer blends and composites can overcome these drawbacks of PLA [17–26].

Poly(butylene adipate-co-terephthalate) (PBAT) is a biodegradable copolymer which can be degraded by microorganisms. PBAT has a superior in ductile property with high elongation at break and excellent in thermal stability [20]. PLA/PBAT blends are highly desirable materials due to high mechanical strength contributed by PLA and elevate in toughness and flexibility obtained from PBAT [18–20]. Therefore, PBAT is considered as a good candidate for enhancing the ductility of PLA [20–24]. Although PBAT is flexible and has superior toughness, it possibly loses dimensional stability during 3D printing [25]. Additionally, most 3D printing technologies require appropriate additives and fillers for controlling the printability and quality of 3D printing products [14]. The addition of fillers could reduce thermal shrinkage, warpage, and curling of the edges of conventional thermoplastic materials [3]. Talc represents one of the most useful mineral fillers for PLA, especially at high temperature service applications. Cicala et al. informed testing results of three different commercial PLA filaments for FDM [14]. The test method in this report was performed by printing a complex shape with overhang features. They found that the best printing quality is observed with the presence of mineral fillers. Zhou et al. studied the preparation of 3D printing from PBS/talc composite filaments. [27]. Several reports revealed that talc acts as the nucleating agent for PLA crystallization. The incorporation of talc increases stiffness and viscosity and improves thermal stability and heat distortion temperature of the composites, which would support dimensional stability in the 3D printing [26–30].

In this study, superior toughened biodegradable polymer blend composites from PLA, PBAT, and nano talc were prepared for alternative materials in 3D printing. Herein, a quality of 3D printable filaments was evaluated by controlled diameter of 1.70 to 1.80 mm. The effects of PBAT and nano talc contents on appearances, surface finish, and properties of dumbbell and overhang 3D printing products were investigated. Mechanical properties were performed by tensile testing. Morphology observation, rheological behaviour, thermal stability, and thermal-induced volume expansion of materials, crystallization, and thermal properties were carried out in order to clarify material characteristics during 3D printing and properties of the final 3D printed products.

Table 1: Formulations of PLA/PBAT blends and PLA/PBAT-nano talc composites.

Materials	Content (wt%)				
PLA	100	90	80	70	60
PBAT	0	10	20	30	40
Nano talc	0 to 40				

Material formulation being referred to in the abbreviations: 90/10-Talc1 = PLA 90 wt%, PBAT 10 wt%, and nano talc 1 wt%.

2. Experimental

2.1. Materials. PLA (Luminy® PLA L175) was supplied by Total Corbion PLA (Thailand) Ltd., with melt flow rate (MFR) 3 g/10 min (190°C, 2.16 kg), glass transition temperature (T_g) 55-60°C, and melting point (T_m) 175°C. PBAT (ecoflex®F Blend C1200) was provided by BASF Japan Ltd., with MFR 2.7-4.9 g/10 min (190°C, 2.16 kg) and T_m 110-120°C. Nano talc (nano ACE, D-800) was supplied by Nippon Talc Co., Ltd., Japan, in powder form, white colour, with an average particle size of 800 nm.

2.2. Preparation of PLA/PBAT Blends and PLA/PBAT-Nano Talc Composites. Materials were dried in an oven at 100°C for at least 6 h. After that, all materials with desired formulation were melted mixing by twin screw extruder (KZW15TW-30MG-NH, Technovel Co., Ltd., Japan, *L*/*D* of screw = 45). The barrel temperatures from the hopper to the die were set at 170-200°C with the screw speed of 100 rpm. The PLA/PBAT blend and the PLA/PBAT-nano talc composite were pelletized by the pelletizer. The formulations of the blends and the composites are shown in Table 1.

2.3. Preparation of 3D Printing Filaments. Pelletized PLA/PBAT blends and PLA/PBAT-nano talc composites were dried at 100°C for at least 6 h. The dried pellets were extruded into a filament by a capillary rheometer (Capilograph 10, Toyo Seiki Seisaku-sho, Ltd., Japan) at a temperature of 180°C and the extrusion speed of 40 mm/min. A circular die was used to prepare 3D printing filaments with a diameter of 1.75 ± 0.05 mm at the constant drawing speed 1.10 m/min.

2.4. Preparation of Injection Molding and 3D Printing Products. The blends and the composites were prepared as a dumbbell specimen by microinjection molding (EP5 Real Mini, Nissei Plastic Industrial Co., Ltd., Japan) at the barrel temperature from 150 to 210°C and the injection speed of 5 mm/sec.

3D printing products with different model structures were fabricated by FDM 3D printer (da Vinci 1.0 Pro, XYZprinting, Inc., Taiwan). The shape and model structures of specimens were designed and exported as standard triangle language (STL) file type in SOLIDWORKS 2017 software. Then it was exported as g-code files for cooperating the FDM printer by XYZware program as shown in Figure 1. In FDM 3D printing, there are many parameters to be

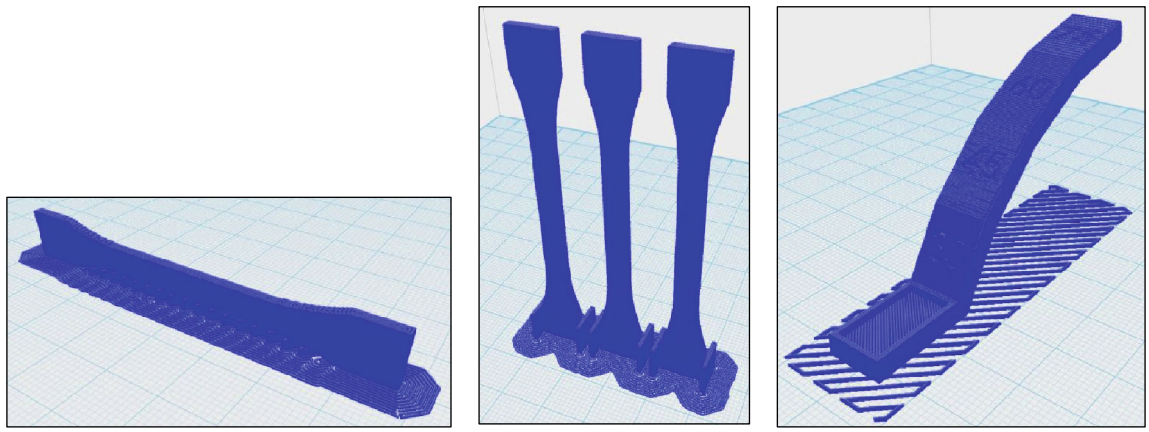

(a) (b) (c)

Figure 1: Software images of 3D printing specimens: (a) horizontal dumbbell; (b) vertical dumbbell; (c) overhang test.

Table 2: Conditions of FDM 3D printing.

Parameters	Conditions
Nozzle temperature	210°C
Bed temperature	45°C
Printing speed	25 mm/s
Infill density	100%
Infill type	Rectilinear
Layer height	0.2 mm
Shell thickness	2 layers
Filament diameter	1.75 ± 0.05 mm
Nozzle size	0.4 mm

controlled carefully such as nozzle temperature, bed temperature, printing speed, infill density, shell thickness, and layer height. In this experiment, details of the printing conditions are shown in Table 2.

2.5. Characterization

2.5.1. Morphology Observation. The samples were fractured after immersion in liquid nitrogen and then coated with platinum. Morphology of the samples was examined by scanning electron microscopy (SEM, JSM-6510, JEOL Ltd., Japan).

The inter layer of the 3D printing products was observed by SEM (TM3030plus, Hitachi, Ltd., Japan) to clarify the relationship between printing behaviour and adhesion characteristic.

2.5.2. Rheological Behaviour. Rheological behaviour of materials was measured by a rotary rheometer (Modular Compact Rheometer, MCR 302, Anton Paar GmbH, Austria). A 25 mm parallel plate was used at the frequency range of 0.01 to 1000 rad/s and the strain set at 1.0%. Complex viscosity (η^*), storage modulus (G'), and loss modulus (G'') were recorded at temperature of 210°C as a function of angular frequency (ω).

2.5.3. Pressure-Volume-Temperature Measurement. Thermal-induced volume expansion of polymers was measured by the pressure-volume-temperature (PVT) system machine (Toyo Seiki Seisaku-sho, Ltd., Japan) at temperature of 30°C to 230°C with constant pressure of 10 MPa.

2.5.4. Thermal Properties and Crystallization. Differential scanning calorimetry (DSC Q200, TA Instruments, USA) was used to analyse thermal properties and crystallization behaviour of materials. Temperature range was set at 40°C to 200°C with heating and cooling rates of 10°C/min. The sample was held isothermally for 5 min to eliminate the thermal history before cooling and the second heating [21].

2.5.5. Precision and Dimension Stability of 3D Printing Products. Precision and dimension stability of 3D printing products were evaluated by performing 3D printing dumbbell shape from vertical printing direction as shown in Figure 1(b). The overhang test specimen was performed to inspect the overhang printing quality [31]. There are 4 levels of protrusion at 30°, 45°, 60°, and 75° as presented in Figure 1(c).

2.5.6. Observation of Surface Roughness. Surface roughness of 3D printing both vertical and horizontal dumbbell specimens was measured by 3D optical surface profiler (NewView 8300, Zygo Corporation, USA) at a middle area of specimen by magnification objective 10x with scan length of 150 μm on the top field area dimension of 1,600 × 1,600 μm^2.

2.5.7. Mechanical Properties. Tensile properties of dumbbell specimen from injection molded and 3D printing products were performed according to ISO 527-2 type 1BA [32] by tensile testing machine (Strograph VG, Toyo Seiki Seisaku-sho, Ltd., Japan) at testing speed of 10 mm/min.

The notched Charpy impact test from injection molded specimen was carried out according to ISO 8256 by a digital impact tester, type DG-IB (Toyo Seiki Seisaku-sho, Ltd., Japan), at potential energy 0.1 J.

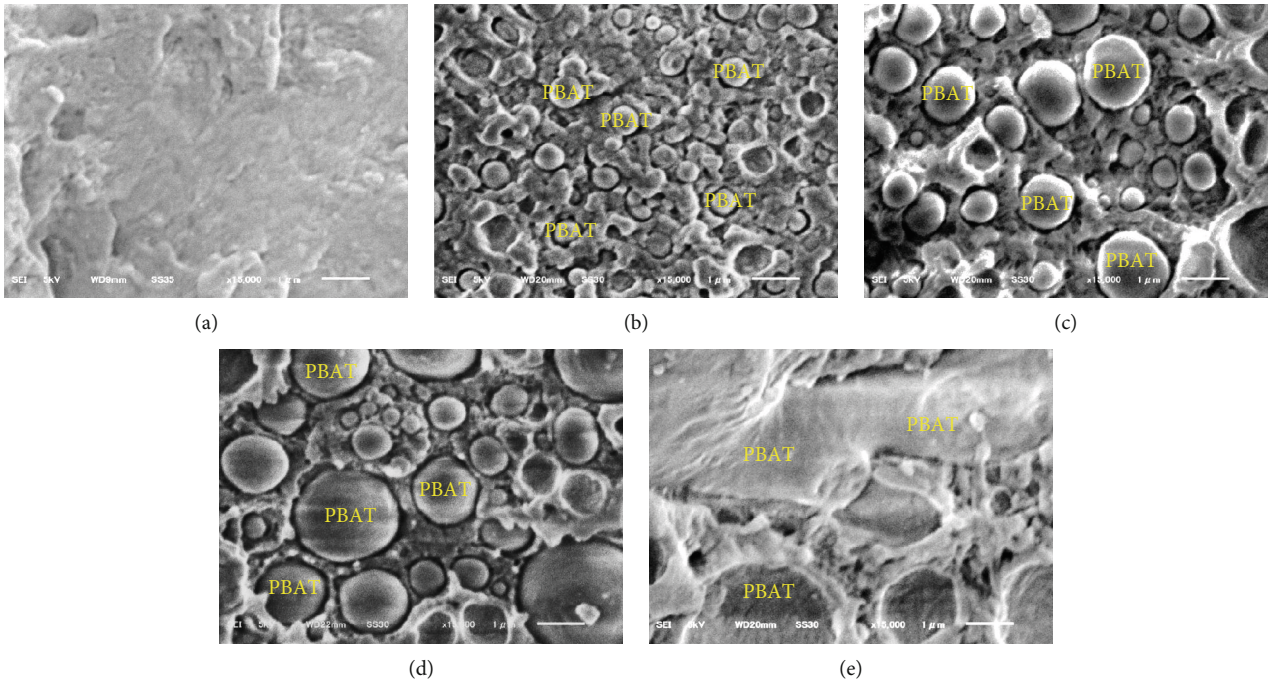

(a) (b) (c) (d) (e)

Figure 2: SEM images of cryogenic fractured surface: (a) 100/0, (b) 90/0, (c) 80/20, (d) 70/30, and (e) 60/40.

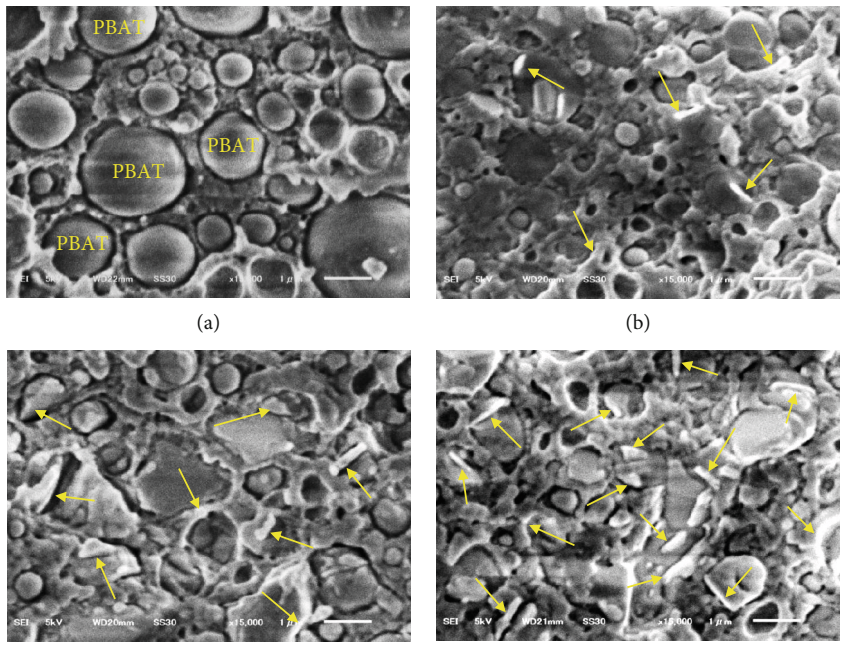

(a) (b) (c) (d)

Figure 3: SEM images of cryogenic fractured surface: (a) 70/30, (b) 70/30-talc1, (c) 70/30-talc5, and (d) 70/30-talc10.

3. Results and Discussion

3.1. Properties of PLA/PBAT Blends and Nano Talc Composites

3.1.1. Morphology of PLA/PBAT Blends and Composites. Morphology of PLA/PBAT blends and 70/30-nano talc composites is shown in Figures 2 and 3, respectively. Figures 2(a)–2(e) present the fractured surface of the PLA/-PBAT blends at PBAT contents 0-40 wt%. It can be seen that PBAT particles were dispersed on the PLA matrix, which indicated that PLA/PBAT was immiscible [33]. The PBAT dispersed phase sizes were in the range of 0.6-1.2 μm, which they became larger when increasing the PBAT contents [33–36]. However, the dispersed phase exhibited cocontinuity

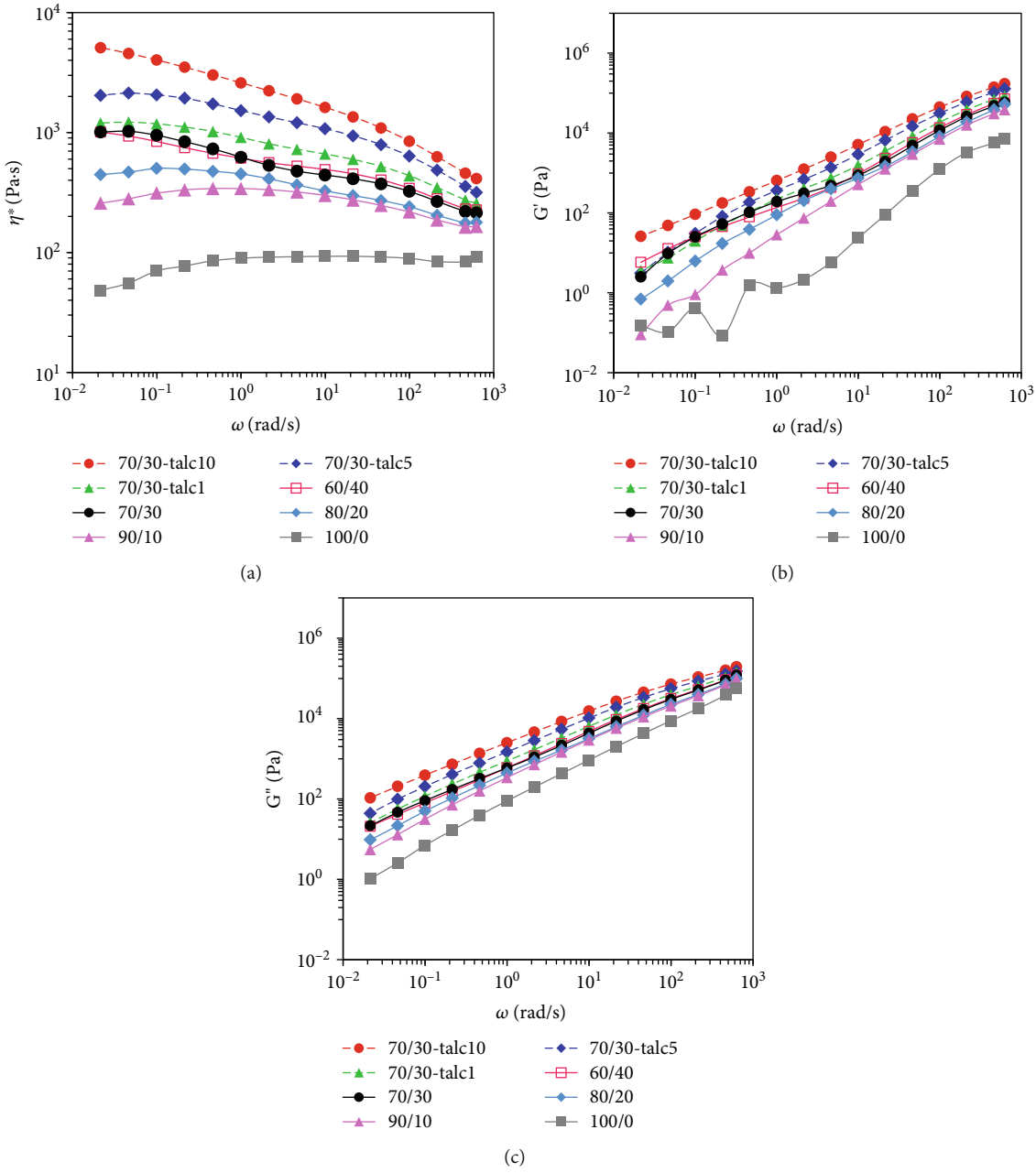

Figure 4: Rheological properties of PLA/PBAT blends and 70/30-nano talc composites: (a) complex viscosity (η^*), (b) storage modulus (G'), and (c) loss modulus (G'').

structures at the content of PBAT 40 wt% as shown in Figure 2(e), which was due to the coalescence of PBAT [33, 34]. Figures 3(a)–3(d) depict the morphology of the 70/30-nano talc composites at the nano talc content 0-10 wt%. It was found that nano talc particles, indicated by arrows in the SEM images, were distributed well on the polymer blend matrix [33]. The PBAT dispersed phase size in the composites became smaller as compared to the 70/30 blend. It was considered that the nano talc particles hindered an agglomeration of PBAT because of an increment of polymer viscosity and surface tension. Hence, the nano talc particles delay the mass transfer during the coalescence of PBAT [33–35].

3.1.2. Rheological Behaviour of PLA/PBAT Blends and Nano Talc Composites. Rheological properties of the blends and the composites are carried out for 3D printing technology in order to determine the printability, dimension stability, and interlayer adhesion in the 3D printing process [7, 18, 27]. Figure 4 illustrates complex viscosity (η^*), storage modulus (G'), and loss modulus (G'') from viscoelastic behaviour of the PLA/PBAT blends and the 70/30-nano talc composites. The complex viscosity as a function of frequency of the PLA/PBAT blends and the composites exhibited pseudoplastic (shear thinning), whereas neat PLA exhibited Newtonian behaviour at higher frequency [18, 27]. The complex viscosity of the blends increased when increasing the

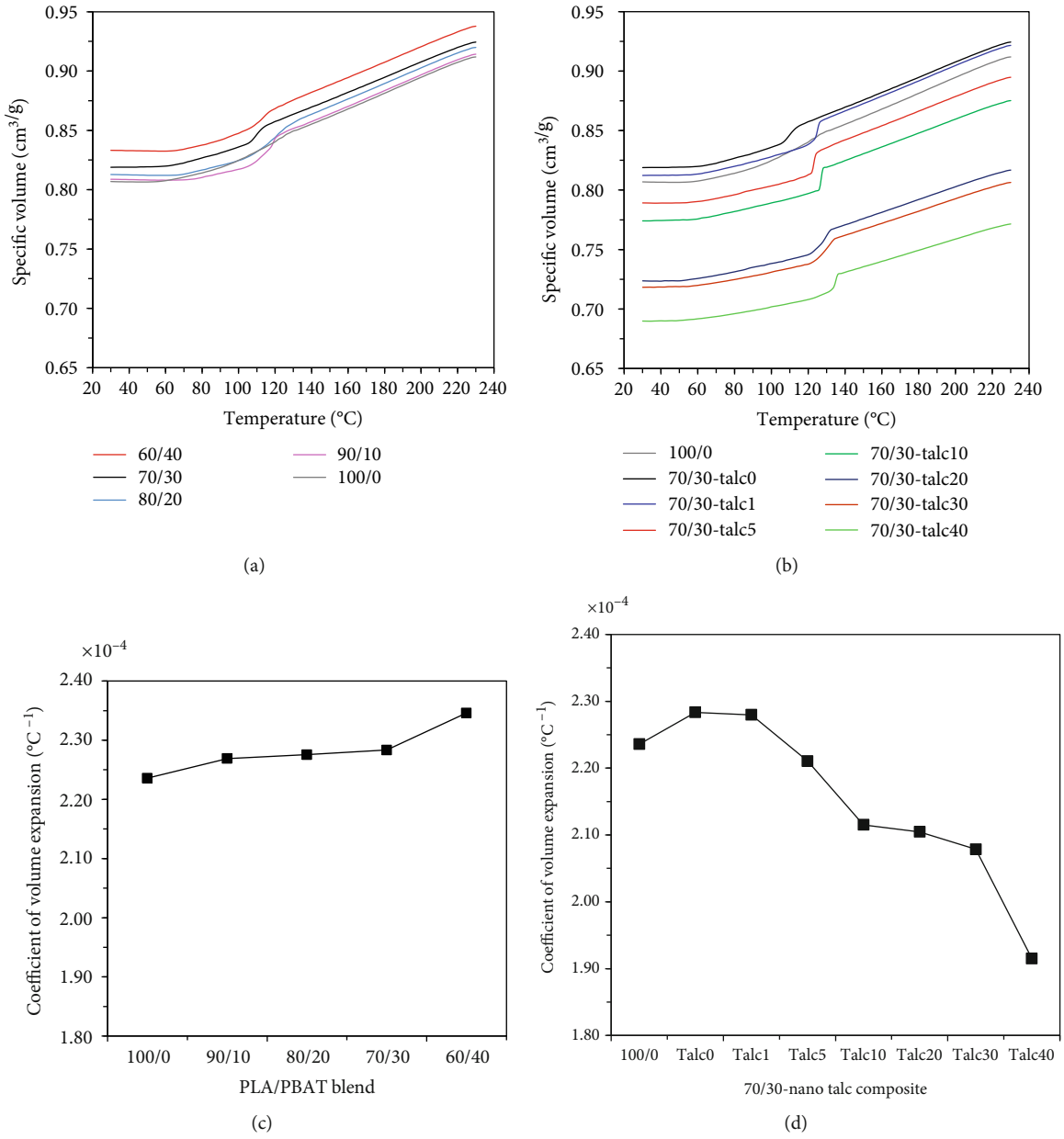

Figure 5: Specific volumes of the (a) PLA/PBAT blend and (b) 70/30-nano talc composite and the coefficients of volume expansion of the (c) PLA/PBAT blend and (d) 70/30-nano talc composite.

PBAT and the nano talc contents as shown in Figure 4(a). Storage modulus and loss modulus of the blends and the composites were also higher than neat PLA as presented in Figure 4(b) and 4(c). It was considered that PBAT has long and flexible molecular chains resulting in elastic deformation due to molecular entanglement [5, 22]. In addition, nano talc inhibited the movement of the polymer chains, which induced stiffness and solid like of molten polymer, especially at low frequency [14, 27, 37–39]. An increment of the storage modulus of the composites informed fine distribution of nano talc and the interaction between nano talc and polymer matrix [5]. Additionally, from Figure 4(b) at low frequency, small plateau of the storage modulus of 70/30 and 60/40 blends indicated changing of elasticity to rubbery flow due to highly entanglement during relaxation process at low frequency [38]. The declination of the complex viscosity and the sudden drop of the storage modulus in neat PLA might be due to deterioration of PLA chain at testing temperature (210°C) [6]. The degree of the complex viscosity would inform printing characteristic. Cicala et al. reported that low viscosity and elasticity of material resulted in flow and dripping of layer deposition that was fallen as poor printing quality [14]. On the contrary, polymers with high viscosities are difficult in printing and lead to inconsistent flow from the nozzle [7]. Qahtani et al. found that their printing job failed due to high viscosity and dimensional instability [6]. Hence,

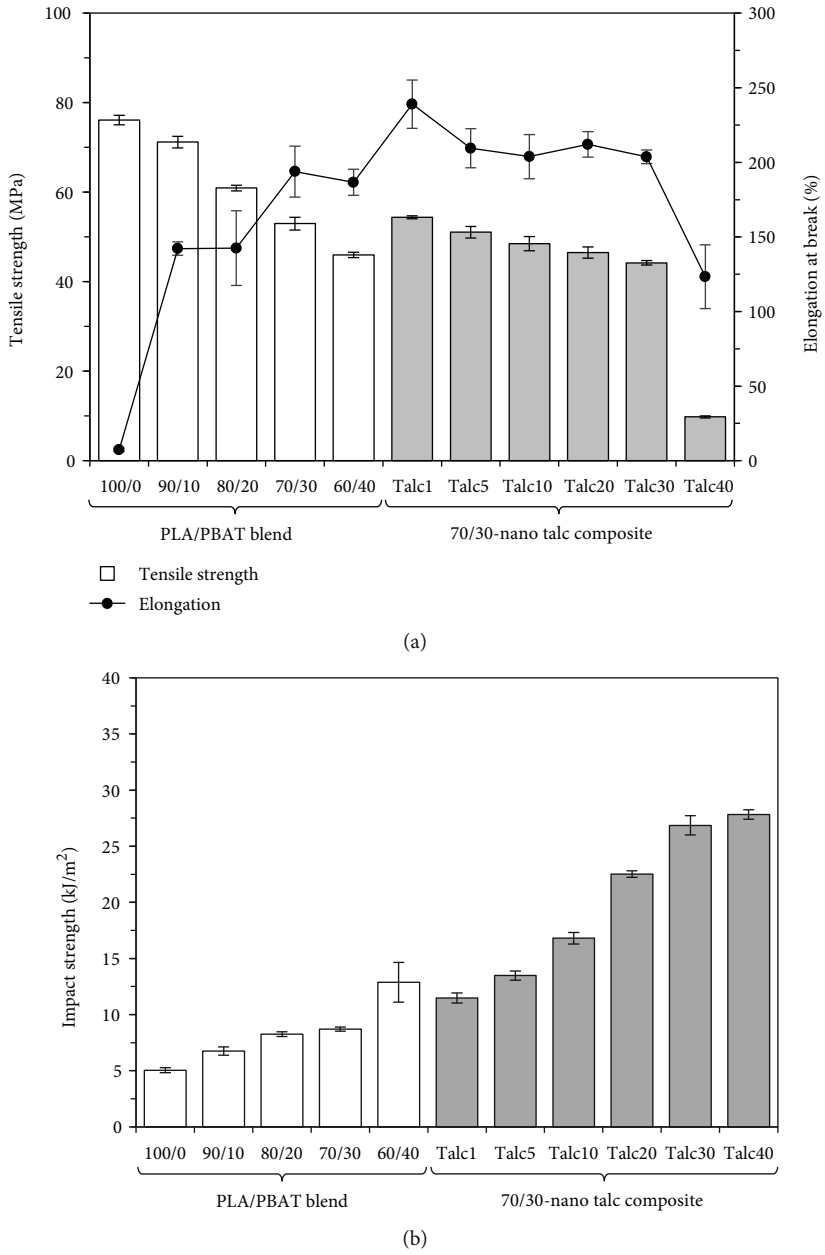

Figure 6: Mechanical properties of PLA/PBAT blends and 70/30-nano talc composites: (a) tensile strength and elongation at break; (b) impact strength.

polymer filament viscosity must be moderate to achieve successful FDM processing conditions [6]. Therefore, the effect of the PBAT and the nano talc contents on the rheological behaviour of the blends and the composites would explain dimension stability of their 3D printing products.

3.1.3. Specific Volume and Coefficient of Volume Expansion. The specific volume of the PLA/PBAT blends and the composites was analysed by PVT measurement at constant pressure with variations of temperatures. Results of the PVT measurement, i.e., the specific volume and the coefficient of volume expansion, are presented in Figure 5. The specific volumes of the blends and the composites rose at elevated temperature as shown in Figures 5(a) and 5(b). The value of the specific volume increased with the incorporation of PBAT as shown in Figure 5(a), which was due to the increment of polymer chains mobility. On the contrary, the addition of nano talc decreased the value of specific volume in the composites, and the value drastically dropped at higher contents of nano talc from 5 wt% to 40 wt% as presented in Figure 5(b). The results indicated that the nano talc restricted polymer chain mobility in the 70/30-nano talc composites during the elevated temperature.

The coefficient of linear thermal expansion (CLTE) and the coefficient of volume expansion can be used for determining dimension changes through printability in the 3D

Table 3: Mechanical properties of PLA/PBAT blends and 70/30-nano talc composites.

PLA/PBAT-nano talc	Tensile strength (MPa)	Young's modulus (GPa)	Elongation at break (%)	Impact strength (kJ/m^2)
100/0-talc0	76.1 ± 2.80	2.3 ± 0.14	7.3 ± 3.30	5.0 ± 0.60
90/10-talc0	71.2 ± 3.10	2.2 ± 0.95	142.2 ± 12.50	6.8 ± 1.09
80/20-talc0	60.9 ± 1.50	2.3 ± 0.06	142.5 ± 54.50	8.2 ± 0.46
70/30-talc0	53.0 ± 3.60	2.0 ± 0.20	193.8 ± 49.60	8.7 ± 0.49
60/40-talc0	46.0 ± 1.70	1.8 ± 0.20	186.6 ± 23.17	12.9 ± 3.86
70/30-talc1	54.4 ± 1.00	2.2 ± 0.30	239.0 ± 45.30	11.5 ± 1.09
70/30-talc5	51.0 ± 3.30	2.2 ± 0.17	209.4 ± 32.20	13.5 ± 1.01
70/30-talc10	48.5 ± 4.38	2.1 ± 0.17	203.9 ± 38.65	16.8 ± 1.25
70/30-talc20	46.5 ± 3.00	2.4 ± 0.17	212.0 ± 20.10	22.5 ± 0.95
70/30-talc30	44.2 ± 1.45	2.6 ± 0.40	203.7 ± 11.10	26.8 ± 2.17
70/30-talc40	9.8 ± 0.06	3.1 ± 0.34	123.3 ± 64.40	27.8 ± 1.17

printing technology [3, 6, 40]. In this research, the coefficient of volume expansion (β) can be estimated from the specific volume as the following equation [40]:

$$\beta = \frac{1}{V}\left(\frac{\Delta V}{\Delta T}\right), \quad (1)$$

where V is a specific volume at room temperature, ΔV is a change in the specific volume due to heating or cooling, and ΔT is temperature differences in the range of the change in the specific volume.

Figures 5(c) and 5(d) display the coefficient of volume expansion of the PLA/PBAT blends and the composites, respectively. The coefficient of volume expansion of the blends increased when increasing the content of PBAT as presented in Figure 5(c). It was considered that PBAT is a long molecule chain that was easily moved during thermal induction, which resulted in higher values of the coefficient of volume expansion [41]. It can be implied that the materials having high thermal-induced volume expansion may dominate thermal instability of molten filament resulting in poor dimension stability, warpage, and shrinkage in the 3D printing products [3, 6]. On the other hand, the coefficient of volume expansion of the composites decreased when increasing the nano talc content as depicted in Figure 5(d). It was due to superior thermal resistance of the nano talc that prevented the expansion of the composites during the elevated temperature [42, 43]. It has been reported that the addition of mineral fillers in 3D printing filaments decreased the coefficient of volume expansion, which contribute for improving printability, reducing warpage, shrinkage, and printing defects in the 3D printing process [3].

3.1.4. Mechanical Properties of Injection Molded Parts. The effects of the PBAT and the nano talc contents on mechanical properties of injection molded parts have been investigated in order to clarify the ratio between the PLA/PBAT blends and the nano talc contents for the 3D printing process. Figure 6 and Table 3 show tensile and impact properties of the PLA/PBAT blends and the composites.

From Figure 6(a) and Table 3, tensile strength and Young's modulus of the PLA/PBAT blends decreased while elongation at break increased when increasing the PBAT content. The declination of tensile strength and Young's modulus and the increment of elongation at break were attributed to high ductility, low modulus, and low tensile strength of PBAT [34, 38]. The maximum elongation at break of 193.8% was found at the 70/30 blend. However, the reduction of the elongation at break in the 60/40 blend might due to larger dispersed phase sizes as well as the cocontinuity structured in the 60/40 PLA/PBAT blend as presented in Figure 2 [34]. From the results, the 70/30 blend was selected to composite with the nano talc.

The effect of the nano talc on mechanical properties of the 70/30-nano talc composites has been discussed. Young's modulus significantly increased with increasing the nano talc contents from 20 wt% to 40 wt% as depicted in Figure 6(a) and Table 3, which was due to the stiffness of the nano talc. At the content of the nano talc 1 wt% to 30 wt%, tensile strength in the composites was lower, whereas elongation at break of the composites was higher than the 70/30 blend. These results were attributed to the less adhesion between the nano talc and the polymer blend matrix and the reduction of PBAT dispersed phase when adding the nano talc in the composites as shown in Figure 3. It is interesting to note that the maximum elongation at break about 239% was observed at the composite with 1 wt% of nano talc. However, the values of both tensile strength and elongation at break were greatly reduced at 40 wt% of nano talc. It was considered that nano talc was highly agglomerated and restricted the movement of polymer chain in the composites and the macro phase separation between the filler and the matrix [44, 45]. The results suggested that the maximum of the nano talc content in the PLA/PBAT composite should be less than 30 wt% for optimizing material properties.

Figure 6(b) depicts the impact strength of the PLA/PBAT blends and the composites. From the result, the impact strength of the blends and the composites increased with increasing the contents of PBAT and nano talc. It was due to the ductility of PBAT and the reduction of PBAT dispersed phases in the blends and the composite [33, 45]. Therefore,

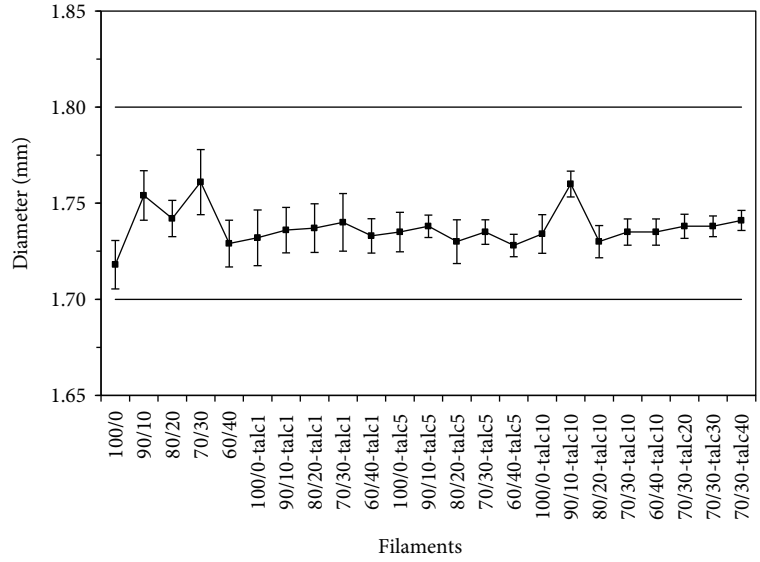

Figure 7: Diameter of 3D printing filaments.

the PLA/PBAT blends and the nano talc composites were able to absorb more energy and performed higher values of the impact strength as compared with neat PLA.

3.2. Production of 3D Printing Filaments. The 3D printing filaments of the PLA/PBAT blends and the nano talc composites were successfully prepared by capillary rheometer (vertical extrusion). The diameter of all filaments can be controlled in the range of 1.75 ± 0.05 mm as shown in Figure 7. The deviation of the diameter was reduced when increasing the nano talc content, which was considered from the increasing in the viscosity and the decreasing of the coefficient of volume expansion in the composites. Therefore, high viscosity and low values of the coefficient of volume expansion were benefits for preparation and control filament diameters especially in the vertical flow of capillary rheometer.

3.3. Properties of 3D Printing Products

3.3.1. Dimension Stability and Printability of the 3D Printing Products. In this study, the PLA/PBAT blends and the 70/30-nano talc composites were neatly printed in the horizontal dumbbell specimen. Hence, the printability and the dimension stability of the 3D printing products were evaluated from the vertical dumbbell and the overhang test specimens as presented in Figures 8 and 9, respectively. From Figure 8, the PLA/PBAT blends can be maintained the shape up to 20 wt% of the PBAT content. The rough surface appeared in the 70/30 blend specimen, and the printing was not completed at the 60/40 blend. It was attributed to the flexibility of PBAT and the high value of the coefficient of volume expansion at printing temperature. Therefore, these specimens exhibited lack of consistency and less dimension accuracy in the printing products. On the contrary, the addition of the nano talc significantly improved the printing of the PLA/PBAT blend composite, especially the 60/40 blend as shown in the bottom line of Figure 8. Cicala et al. reported that mineral fillers act as reinforcement in printed parts that kept their shape during printing [14]. In addition, Figure 9 shows the effect of the nano talc contents on the overhang test products in the 70/30-nano talc composites. The results revealed that the dimension stability of the 3D printing products of the 70/30 composite was successfully improved when increasing the nano talc content. It can be noted that the composite printing products were possible to be produced even in the angle up to 75° for the overhang test without a supporter, which is better than a conventional standard at 45° of design rules for the FDM 3D printing [14, 31]. The incorporation of the nano talc in the 70/30 blend depicted the improvement of dimension stability as well as surface characteristic. It was due to the reinforcement of the nano talc, the increment of the viscosity, and the reduction of the coefficient of volume expansion in order to control the stability of the molten filament [3, 6, 14, 27].

3.3.2. Thermal Properties and Crystallization Behaviour of the 3D Printing Products. Figure 10 illustrates DSC thermograms of the PLA/PBAT blends and the 70/30-nano talc composites at the nano talc content 1-10 wt%. Results of glass transition temperature (T_g), cold crystallization temperature (T_{cc}), melting temperature (T_m), crystallization temperature (T_c), enthalpy of cold crystallization (ΔH_{cc}), enthalpy of melting (ΔH_m), and degree of crystallinity (X_c) of the 3D printing products from the cooling cycle and the second heating are tabulated in Table 4. The degree of crystallinity was calculated based on the following equation [17, 18]:

$$X_c\,(\%) = \frac{\Delta H_m - \Delta H_{cc}}{\Delta H_f^0} \times \frac{1}{W} \times 100, \quad (2)$$

where ΔH_m is the enthalpy of melting, ΔH_{cc} is the enthalpy of cold crystallization, $\Delta H^0{}_f$ is the heat of fusion for fully crystalline PLA 93.7 J/g [18], and W is the weight fraction of PLA in the PLA/PBAT blends and the composites.

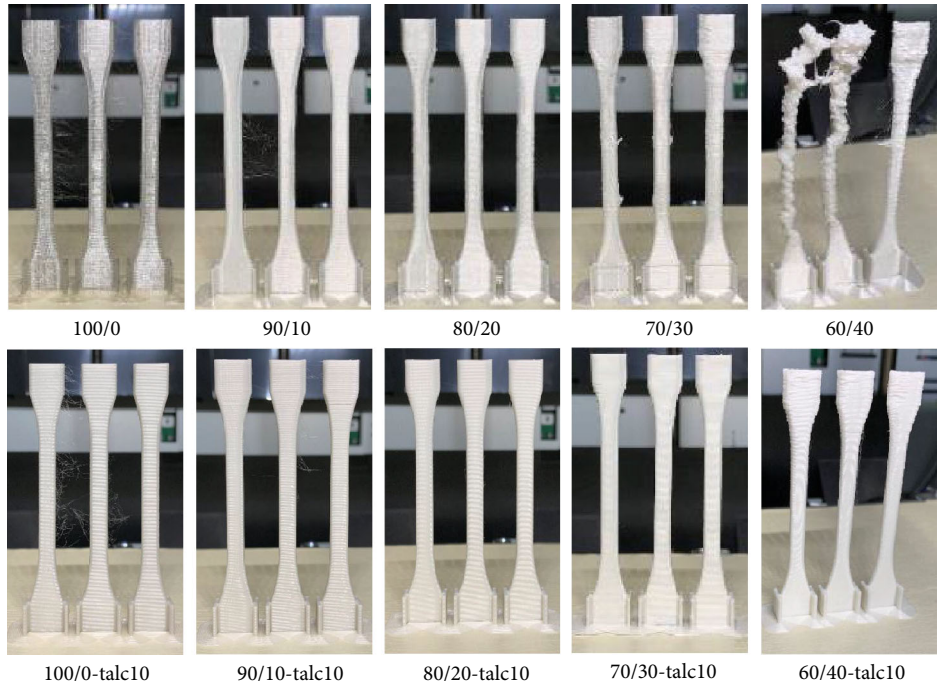

Figure 8: Photographs of vertical dumbbell 3D printing specimens.

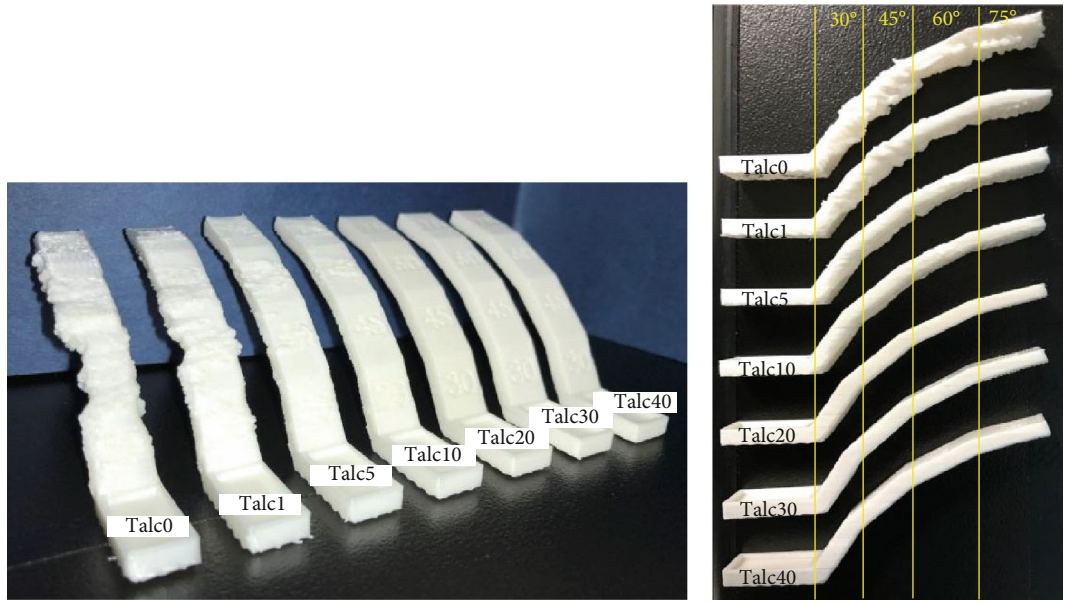

Figure 9: Overhang test specimens of 70/30-nano talc composites.

Figures 10(a) and 10(b) depict DSC thermograms from the first heating of the PLA/PBAT blends and the composites, respectively. The cold crystallization in the blends and the composites can be observed, which indicated that the polymer chain does not have enough time for organizing and ordering polymer molecules to crystallize during printing products. However, the addition of the nano talc decreased the cold crystallization temperature in the 70/30-nano talc composites in which the nano talc promoted the crystallization in the composites. The results were confirmed by sharper of the crystallization temperature in the composites as compared to the PLA/PBAT blends as shown in the cooling cycle in Figures 10(c) and 10(d). Furthermore, the cold crystallization existed in the blends while it disappeared in the composites in the second heating as depicted in Figures 10(e) and 10(f), respectively.

Table 4 summarizes thermal properties of the blends and the composites from the cooling cycle and the second

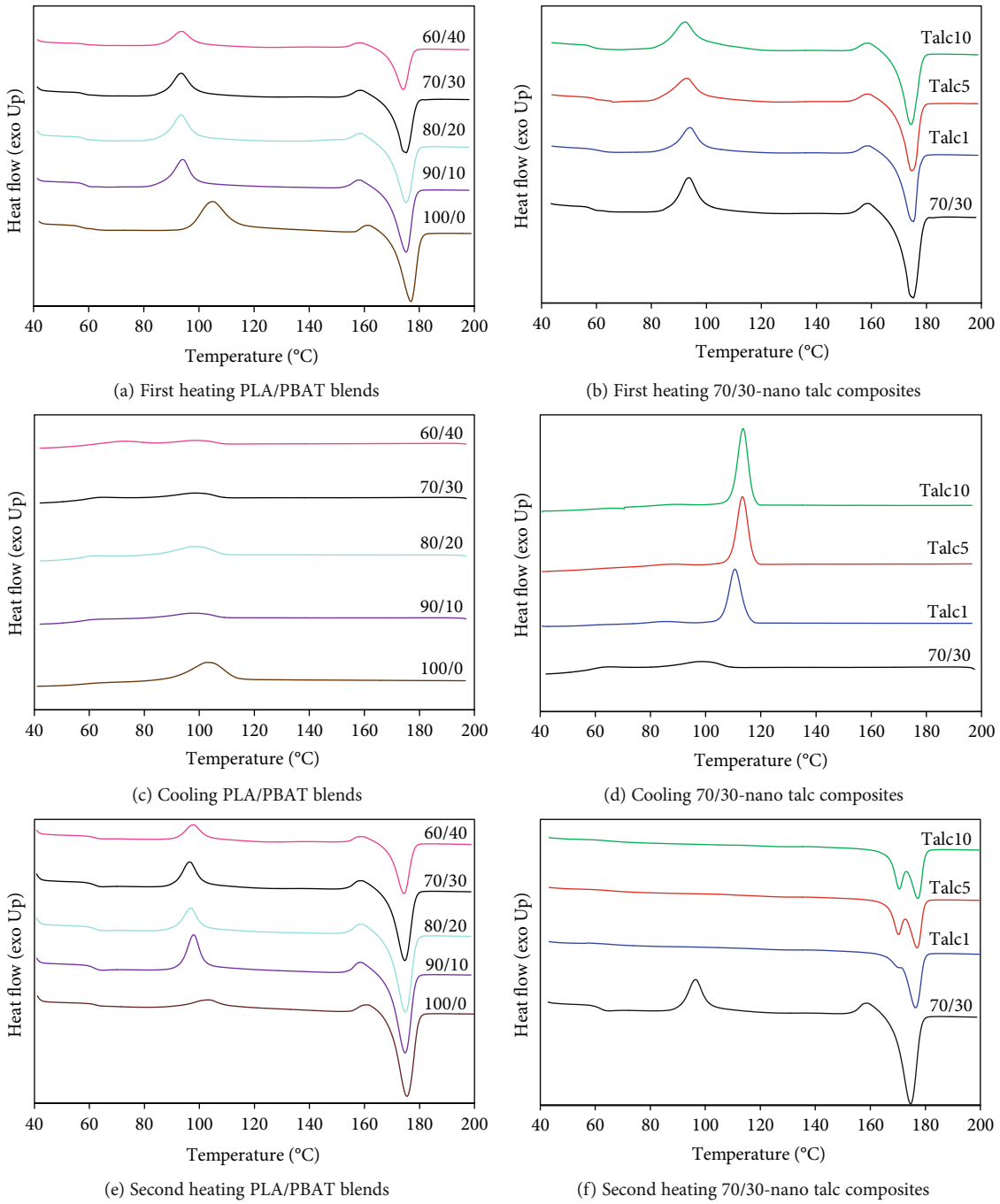

(a) First heating PLA/PBAT blends

(b) First heating 70/30-nano talc composites

(c) Cooling PLA/PBAT blends

(d) Cooling 70/30-nano talc composites

(e) Second heating PLA/PBAT blends

(f) Second heating 70/30-nano talc composites

Figure 10: DSC thermograms of 3D printing specimens.

heating. The crystallization temperature of PLA in the blends was low in which PBAT retarded the crystallization of PLA during printing. On the other hand, the incorporation of the nano talc increased crystallization temperature of PLA in the composites, and the cold crystallization was vanished in the composites. The results implied that the nano talc improved the PLA crystallization in the 70/30-nano talc composites, which confirmed by higher degree of crystallinity of PLA in the composites than in the blends. It was considered that the nano talc acted as the heterogeneous nucleation site while PBAT dispersed phase retarded for PLA to crystallize [44–49]. Double peaks of the melting endotherm in the composites after printing as presented in Figure 10(d) indicated partial melting, recrystallization, and remelting of crystal in the composites [38, 45, 49]. The increment of the glass transition temperature of PLA in the composites informed the restriction of polymer chain mobility because of the addition of the nano talc. It can be noted that the increasing of the crystallization temperature and the glass transition temperature of PLA in the composites notified faster solidification of molten polymer and reinforcing of the printing products, respectively.

Table 4: Thermal properties of PLA/PBAT blends and composites.

PLA/PBAT-nano talc	T_c (°C)	T_g (°C)	T_{cc} (°C)	ΔH_{cc} (J/g)	PLA $T_{m\,peak1}$ (°C)	PLA $T_{m\,peak2}$ (°C)	ΔH_m (J/g)	X_c (%)
100/0	102.6	60.0	103.4	11.2	—	175.4	46.6	37.8
90/10	97.5	59.3	97.6	24.0	—	174.7	41.2	20.4
80/20	98.0	59.7	96.8	16.0	—	174.8	35.1	25.5
70/30	98.6	59.7	96.4	17.0	—	174.7	30.8	21.0
60/40	99.1	59.6	97.8	13.4	—	174.2	26.4	23.1
70/30-talc1	110.5	62.5	—	—	—	176.4	32.1	49.5
70/30-talc5	113.3	63.1	—	—	170.2	176.9	31.2	49.9
70/30-talc10	113.6	64.3	—	—	170.6	177.3	29.3	49.2
70/30-talc20	114.6	61.2	—	—	170.0	176.7	29.4	53.7
70/30-talc30	114.7	61.9	—	—	170.2	176.6	27.4	54.3
70/30-talc40	115.6	60.1	—	—	170.4	176.7	26.2	56.0

3.3.3. Surface Roughness of the 3D Printing Products. Figure S1 presents the scanning profile of the surface roughness measurement. The 3D surface roughness data was evaluated as the surface roughness average (R_a) by Zygo Mx software according to Equation S1 [50]. Surface roughness average (R_a) of the vertical and the horizontal dumbbell specimens is presented in Figures 11(a) and 11(b) for the PLA/PBAT blends and the 70/30-nano talc composites, respectively. At the vertical printing direction, the surface roughness significantly increased when increasing the PBAT content in the blends while drastically decreased with the addition of the nano talc in the 70/30-nano talc composites. According to the PLA/PBAT blends, the volume of molten polymer in the blends increased at the printing condition as observed from high values of the coefficient of volume expansion in the blends. Therefore, the molten filament was instability, and the printed layers of the blends have less time to solidify completely before the next printing level resulted in surfaced defect in the vertical specimen [2, 50, 51]. At the horizontal printing direction, the surface roughness of the blends and the composites was lower than the neat PLA and the PLA commercial filament ($R_a = 20.7\,\mu$m). The surface roughness decreased when increasing the content of PBAT in Figure 11(a), whereas it almost unchanged when adding the nano talc in Figure 11(b). It was considered that the melted layers have time for adhered and solidified layer by layer in the horizontal printing direction. Hence, the surfaces of the horizontal specimens were smooth. It can be noted that the PBAT and the nano talc improved the dimensional accuracy and the surface quality of these horizontal specimens [50, 51].

3.3.4. Adhesion between Interlayers. Since molten polymer is fabricated layer by layer in 3D printing, an integrity of adhesion between the layers is required in order to enhance mechanical properties of 3D printing products [6]. The bonding between layers of FDM parts is driven by the thermal energy of the semimolten material [9]. Figure S2 shows the schematic observation of interlayer and voids from cross-sectional vertical dumbbell specimen. Figures S3 and S4 present SEM images of alignment layers in the PLA/PBAT blends and the 70/30-nano talc composites, respectively. Figure 12 depicts SEM images of the interlayers in the PLA/PBAT blends and the 70/30-nano talc composites at high magnification. Voids, which are indicated by arrows, can be observed between layers in neat PLA, the blends and the composites. Sizes of the voids obviously decreased with adding higher contents of PBAT as shown in Figures 12(a)–12(c), which provides larger contact area in the blends [8]. On the contrary, the sizes of the voids increased when increasing the nano talc contents as presented in Figures 12(d)–12(f). The result was considered that the reduction of the voids was due to higher values of the coefficient of volume expansion of PLA/PBAT blends. Thus, the melted layers were easily adhered during printing and continuing immersed layer by layer when increasing the PBAT contents. On the other hand, the voids between layers increased with increasing the nano talc contents. Since the adding of nano talc increased the viscosity, reduced the coefficient of volume expansion, and enhanced the crystallization temperature of the composites, the diffusion of polymer molecular chain was retarded, and between layers were solidified faster resulting in the reduction of filaments welding, which exhibited larger voids and lack of interlayer adhesion [3, 8, 14, 50].

3.3.5. Tensile Properties of the 3D Printing Products. Tensile properties of the 3D printed dumbbell specimens are shown in Table 5. Tensile strength of the blends and the composites decreased in both of horizontal and vertical dumbbell specimens with increasing the PBAT and the nano talc contents. It was owing to the ductility of the PBAT and less adhesion between the nano talc and the polymer matrix. The elongation at break of the blends and the composites increased when increasing the contents of PBAT and nano talc, which was accounted to the reduction of PBAT dispersed phase sizes and the orientation of printed layer in the horizontal specimens. However, the elongation at break of the composites with horizontal printing decreased at high nano talc contents because of the cluster of the nano talc in the composites. On the contrary, the blends and the composites at the vertical printing direction were difficult to elongate because of poor adhesion between the printed layers, which

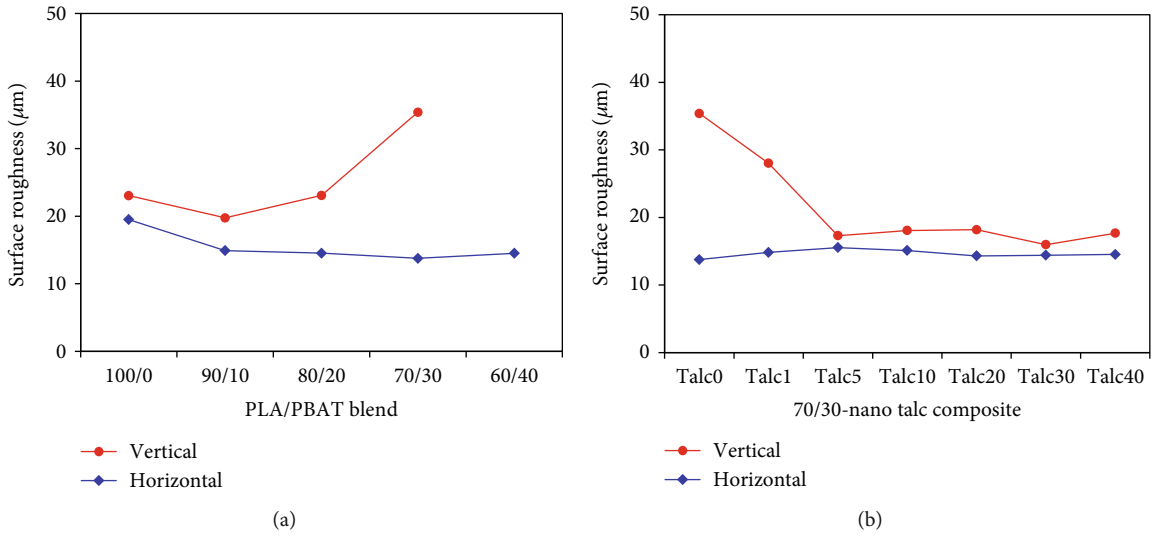

Figure 11: Surface roughness of vertical and horizontal dumbbell specimens: (a) PLA/PBAT blends; (b) 70/30-nano talc composites.

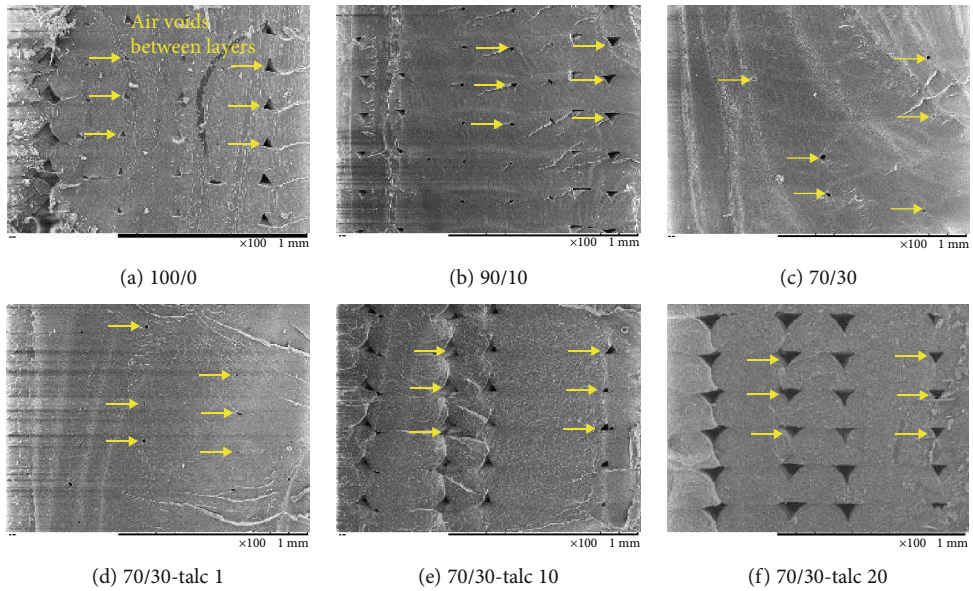

Figure 12: SEM images of cross-sectional surface of vertical dumbbell specimens (examples of air voids are located by arrows).

might be implied from the tensile strength of the vertical dumbbell specimens [2]. From the horizontal printing direction, tensile strength of these systems was comparable to products from commercial available filaments. Additionally, the elongation of the PLA/PBAT blends and the composites was higher than the products from the commercial as tabulated in Table 5. From the results, 3D printable filaments prepared in this study were comparable to use in FDM 3D printing technology.

4. Conclusion

It was suggested that the novel superior toughened 3D printable filaments of the PLA/PBAT-nano talc composites were successfully prepared, showing the excellent dimensional stability and printability, and presented high tensile properties of printing products as compared with neat PLA and the commercial 3D printing filaments. The nano talc plays the key role in the production of 3D printing products. The complex viscosity, crystallization temperature, and degree of crystallization of the composites increased while the coefficient of volume expansion decreased with the addition of the nano talc in the 70/30-nano talc composites, resulting in the improvement of dimension stability, surface roughness, and elongation at break of the composites. It was possible to print the PLA/PBAT-nano talc filaments even at the angle up to 75° during the overhang test without a supporter. However, 3D pintable filaments with nano talc contents

Table 5: Tensile properties of the blends and the composite 3D specimens and the commercial data* [52–58].

No.	Materials	Horizontal		Vertical	
		Tensile strength (MPa)	Elongation at break (%)	Tensile strength (MPa)	Elongation at break (%)
1	100/0	57.9 ± 5.53	3.6 ± 0.15	34.4 ± 3.20	2.4 ± 0.20
2	90/10	55.8 ± 4.00	4.1 ± 0.80	30.1 ± 2.11	1.9 ± 0.10
3	80/20	54.2 ± 4.80	7.0 ± 2.10	25.6 ± 2.30	1.8 ± 0.10
4	70/30	46.9 ± 2.00	225.8 ± 25.90	19.4 ± 1.90	1.6 ± 0.20
5	60/40	39.7 ± 2.30	348.4 ± 41.80	11.3 ± 1.80	1.8 ± 0.60
6	70/30-talc1	45.3 ± 3.10	410.0 ± 44.60	20.6 ± 2.10	2.2 ± 0.30
7	70/30-talc5	46.3 ± 2.90	348.5 ± 39.10	19.5 ± 1.10	2.0 ± 0.20
8	70/30-talc10	41.7 ± 3.50	177.4 ± 31.00	16.2 ± 0.50	1.7 ± 0.20
9	70/30-talc20	40.2 ± 2.00	104.7 ± 19.50	14.2 ± 2.00	1.5 ± 0.20
10	70/30-talc30	39.1 ± 3.10	44.1 ± 15.40	13.0 ± 1.20	1.1 ± 0.00
11	70/30-talc40	38.6 ± 1.10	22.0 ± 13.80	12.0 ± 1.70	1.0 ± 0.11
12	PLA (Ultimaker)*	49.5	5.2	—	—
13	ABS (Ultimaker)*	39.0	4.8	—	—
14	PolyMax™ PLA (Polymaker)*	28.1	1.4	—	—
15	PolyLite™ PLA (Polymaker)*	46.6	1.9	—	—
16	PolyLite™ ABS (Polymaker)*	33.3	2.7	—	—
17	ECOMAX® PLA (3DXTECH)*	56.0	8.0	—	—
18	3DXMAX® ABS (3DXTECH)*	42.0	10.0	—	—
19	Innofil3D PLA (BASF)*	38.1	2.8	28.8	1.1
20	Innofil3D ABS (BASF)*	29.3	3.7	6.5	0.7

*Tensile properties of the commercial data, horizontal printed in x, y-axis and vertical printed in z-axis [52–58].

more than 10 wt% presented excellent dimension stability but exhibited a lack of tensile properties. In this study, the optimum formulation of PLA/PBAT-nano talc 3D printable filaments should be in the range of PBAT 10 wt% to 30 wt% and the content of nano talc 1 wt% to 10 wt%.

Data Availability

The data used to support the findings of this study are available from the corresponding author upon request.

Conflicts of Interest

The authors declare no conflict of interest.

Acknowledgments

This research was financially supported by JSPS Grant-in-Aid for Scientific Research on Innovative Areas Grant Number JP18H05483. The authors would like to give thanks for the support of the doctoral scholarship from Pathumwan Institute of Technology, Thailand, for Mr. Wattanachai Prasong.

Supplementary Materials

Figure S1: scanning profile of surface roughness measurement. Figure S2: schematic observation of interlayer and voids from cross-sectional vertical dumbbell specimen. Figure S3: SEM images of alignment layers in the PLA/PBAT blends. Figure S4: SEM images of alignment layers in the 70/30-nano talc composites. *(Supplementary Materials)*

References

[1] S. C. Ligon, R. Liska, J. Stampfl, M. Gurr, and R. Mülhaupt, "Polymers for 3D printing and customized additive manufacturing," *Chemical Reviews*, vol. 117, no. 15, pp. 10212–10290, 2017.

[2] Q. Ou-Yang, B. Guo, and J. Xu, "Preparation and characterization of poly(butylene succinate)/polylactide blends for fused deposition modeling 3D printing," *ACS Omega*, vol. 3, no. 10, pp. 14309–14317, 2018.

[3] S. H. Kochesfahani, *Improving PLA-based material for FDM 3D-printers using minerals (principles and method development)*, SPE ANTEC™ Indianapolis, 2016.

[4] I. Chiulan, A. Frone, C. Brandabur, and D. Panaitescu, "Recent advances in 3D printing of aliphatic polyesters," *Bioengineering*, vol. 5, no. 1, p. 2, 2018.

[5] W. Xu, A. Pranovich, P. Uppstu et al., "Novel biorenewable composite of wood polysaccharide and polylactic acid for three dimensional printing," *Carbohydrate Polymers*, vol. 187, pp. 51–58, 2018.

[6] M. Qahtani, F. Wu, M. Misra, S. Gregori, D. F. Mielewski, and A. K. Mohanty, "Experimental design of sustainable 3D-printed poly(lactic acid)/biobased poly(butylene succinate)

blends via fused deposition modeling," *ACS Sustainable Chemistry & Engineering*, vol. 7, no. 17, pp. 14460–14470, 2019.

[7] E. V. Diederichs, M. C. Picard, B. P. Chang, M. Misra, D. F. Mielewski, and A. K. Mohanty, "Strategy to improve printability of renewable resource-based engineering plastic tailored for FDM applications," *ACS Omega*, vol. 4, no. 23, pp. 20297–20307, 2019.

[8] N. Aliheidari, J. Christ, R. Tripuraneni, S. Nadimpalli, and A. Ameli, "Interlayer adhesion and fracture resistance of polymers printed through melt extrusion additive manufacturing process," *Materials and Design*, vol. 156, pp. 351–361, 2018.

[9] C. Bellehumeur, L. Li, Q. Sun, and P. Gu, "Modeling of Bond Formation Between Polymer Filaments in the Fused Deposition Modeling Process," *Journal of Manufacturing Processes*, vol. 6, no. 2, pp. 170–178, 2004.

[10] T. Andrew and U. Ertu, *3D Printing- Media Hype or Manufacturing Reality: Textiles Surface Fashion Product Architecture*, Textile Centre of Excellence, Huddersfield UK, 2014.

[11] M. Xia and J. Sanjayan, "Method of formulating geopolymer for 3D printing for construction applications," *Materials and Design*, vol. 110, pp. 382–390, 2016.

[12] B. Coppola, N. Cappetti, L. di Maio, P. Scarfato, and L. Incarnato, "3D printing of PLA/clay nanocomposites: influence of printing temperature on printed samples properties," *Materials*, vol. 11, no. 10, p. 1947, 2018.

[13] N. Mohan, P. Senthil, S. Vinodh, and N. Jayanth, "A review on composite materials and process parameters optimisation for the fused deposition modelling process," *Virtual and Physical Prototyping*, vol. 12, no. 1, pp. 47–59, 2017.

[14] G. Cicala, D. Giordano, C. Tosto, G. Filippone, A. Recca, and I. Blanco, "Polylactide (PLA) filaments a biobased solution for additive manufacturing: correlating rheology and thermomechanical properties with printing quality," *Materials*, vol. 11, no. 7, p. 1191, 2018.

[15] M. A. Cuiffo, J. Snyder, A. M. Elliott, N. Romero, S. Kannan, and G. P. Halada, "Impact of the fused deposition (FDM) printing process on polylactic acid (PLA) chemistry and structure," *Applied Sciences*, vol. 7, no. 6, p. 579, 2017.

[16] C. B. Sweeney, B. A. Lackey, M. J. Pospisil et al., "Welding of 3D-printed carbon nanotube–polymer composites by locally induced microwave heating," *Science Advances*, vol. 3, no. 6, e1700262, 2017.

[17] J. Wootthikanokkhan, T. Cheachun, N. Sombatsompop et al., "Crystallization and thermomechanical properties of PLA composites: effects of additive types and heat treatment," *Journal of Applied Polymer Science*, vol. 129, no. 1, pp. 215–223, 2013.

[18] C. Benwood, A. Anstey, J. Andrzejewski, M. Misra, and A. K. Mohanty, "Improving the impact strength and heat resistance of 3D printed models: structure, property, and processing correlationships during fused deposition modeling (FDM) of poly(lactic acid)," *ACS Omega*, vol. 3, no. 4, pp. 4400–4411, 2018.

[19] Y. Ding, W. Feng, B. Lu, P. Wang, G. Wang, and J. Ji, "PLA-PEG-PLA tri-block copolymers: effective compatibilizers for promotion of the interfacial structure and mechanical properties of PLA/PBAT blends," *Polymer*, vol. 146, pp. 179–187, 2018.

[20] H. Moustafa, N. el Kissi, A. I. Abou-Kandil, M. S. Abdel-Aziz, and A. Dufresne, "PLA/PBAT bionanocomposites with antimicrobial natural rosin for green packaging," *ACS Applied Materials & Interfaces*, vol. 9, no. 23, pp. 20132–20141, 2017.

[21] W. Liu, P. Chen, X. Wang, F. Wang, and Y. Wu, "Effects of poly(butyleneadipate-co-terephthalate) as a macromolecular nucleating agent on the crystallization and foaming behavior of biodegradable poly(lactic acid)," *Cellular Polymers*, vol. 36, no. 2, pp. 75–96, 2017.

[22] D. Nakayama, F. Wu, A. K. Mohanty, S. Hirai, and M. Misra, "Biodegradable composites developed from PBAT/PLA binary blends and silk powder: compatibilization and performance evaluation," *ACS Omega*, vol. 3, no. 10, pp. 12412–12421, 2018.

[23] E. Quero, A. J. Müller, F. Signori, M. B. Coltelli, and S. Bronco, "Isothermal cold-crystallization of PLA/PBAT blends with and without the addition of acetyl tributyl citrate," *Macromolecular Chemistry and Physics*, vol. 213, no. 1, pp. 36–48, 2012.

[24] M. Hernández-López, Z. N. Correa-Pacheco, S. Bautista-Baños et al., "Bio-based composite fibers from pine essential oil and PLA/PBAT polymer blend. Morphological, physicochemical, thermal and mechanical characterization," *Macromolecular Chemistry and Physics*, vol. 234, pp. 345–353, 2019.

[25] S. Singamneni, D. Smith, M. J. LeGuen, and D. Truong, "Extrusion 3D printing of polybutyrate-adipate-terephthalate-polymer composites in the pellet form," *Polymers*, vol. 10, no. 8, p. 922, 2018.

[26] D. Battegazzore, S. Bocchini, and A. Frache, "Crystallization kinetics of poly(lactic acid)-talc composites," *Express Polymer Letters*, vol. 5, no. 10, pp. 849–858, 2011.

[27] Y. Zhou, X. Xia, X. Liu et al., "Preparation and rheological and mechanical properties of poly(butylene succinate)/talc composites for material extrusion additive manufacturing," *Macromolecular Materials and Engineering*, vol. 304, no. 7, 2019.

[28] M. Murariu and P. Dubois, "PLA composites: from production to properties," *Advanced Drug Delivery Reviews*, vol. 107, pp. 17–46, 2016.

[29] F. Yu, T. Liu, X. Zhao, X. Yu, A. Lu, and J. Wang, "Effects of talc on the mechanical and thermal properties of polylactide," *Journal of Applied Polymer Science*, vol. 125, no. S2, pp. E99–E109, 2012.

[30] S. Saravana, G. Bheemaneni, and R. Kandaswamy, "Effect of polyethylene glycol on mechanical, thermal, and morphological properties of talc reinforced polylactic acid composites," *Materials Today: Proceedings*, vol. 5, no. 1, pp. 1591–1598, 2018.

[31] B. Redwood, F. Schöffer, and B. Garret, *The 3D Printing Handbook: Technologies, Design and Applications*, 3D HUBS, 2017.

[32] G. Ćwikła, C. Grabowik, K. Kalinowski, I. Paprocka, and P. Ociepka, "The influence of printing parameters on selected mechanical properties of FDM/FFF 3D-printed part," *Materials Science and Engineering*, vol. 227, 2017.

[33] A. Teamsinsungvon, Y. Ruksakulpiwat, and K. Jarukumjorn, "Poly(lactic acid)/Poly(butylene adipate-*co*-terephthalate) Blend and its Composite: Effect of Maleic Anhydride Grafted Poly(lactic acid) as a Compatibilizer," *Advanced Materials Research*, vol. 410, pp. 51–54, 2011.

[34] Y. Deng, C. Yu, P. Wongwiwattana, and N. L. Thomas, "Optimising ductility of poly(lactic acid)/poly(butylene adipate-co-terephthalate) blends through co-continuous phase morphology," *Journal of Polymers and the Environment*, vol. 26, no. 9, pp. 3802–3816, 2018.

[35] A. L. P. D. L. Freitas, L. R. Tonini Filho, P. S. Calvão, and A. M. C. de Souza, "Effect of montmorillonite and chain extender on rheological, morphological and biodegradation behavior of PLA/PBAT blends," *Polymer Testing*, vol. 62, pp. 189–195, 2017.

[36] L. C. Arruda, M. Magaton, R. E. S. Bretas, and M. M. Ueki, "Influence of chain extender on mechanical, thermal and morphological properties of blown films of PLA/PBAT blends," *Polymer Testing*, vol. 43, pp. 27–37, 2015.

[37] S.-Y. Gu, K. Zhang, J. Ren, and H. Zhan, "Melt rheology of polylactide/poly(butylene adipate- *co* -terephthalate) blends," *Carbohydrate Polymers*, vol. 74, no. 1, pp. 79–85, 2008.

[38] L. Jiang, M. P. Wolcott, and J. Zhang, "Study of biodegradable polylactide/poly(butylene adipate-co-terephthalate) blends," *Biomacromolecules*, vol. 7, no. 1, pp. 199–207, 2006.

[39] R. Al-Itry, K. Lamnawar, and A. Maazouz, "Biopolymer blends based on poly (lactic acid): shear and elongation rheology/-structure/blowing process relationships," *Polymers*, vol. 7, no. 5, pp. 939–962, 2015.

[40] E. J. Padilha Júnior, R. . P. Soares, and N. S. M. Cardozo, "Analysis of equations of state for polymers," *Polímeros*, vol. 25, no. 3, pp. 277–288, 2015.

[41] D. Tripathi and T. K. Dey, "Thermal conductivity, coefficient of linear thermal expansion and mechanical properties of LDPE/Ni composites," *Indian Journal of Physics*, vol. 87, no. 5, pp. 435–445, 2013.

[42] M. Katayama, J. Nakakuki, J.-H. Pee, and Y. Kobayashi, "Effect of particle size of tabular talc powders on crystal orientation and sintering of cordierite ceramics," *Journal of the Ceramic Society of Japan*, vol. 121, no. 1419, pp. 934–939, 2013.

[43] G. Chen, D. Zhiwei, X. Lei, S. Guo, and G. Li, "Modification of a theoretical model for the prediction of the thermal expansion behavior of particulate composites: application to poly(vinyl chloride)/talc composites," *Journal of Macromolecular Science, Part B*, vol. 52, no. 9, pp. 1309–1321, 2013.

[44] A. Shakoor and N. L. Thomas, "Talc as a nucleating agent and reinforcing filler in poly(lactic acid) composites," *Polymer Engineering and Science*, vol. 54, no. 1, pp. 64–70, 2014.

[45] C. Xu, X. Zhang, X. Jin, S. Nie, and R. Yang, "Study on mechanical and thermal properties of poly(lactic acid)/poly(-butylene adipate-co-terephthalate)/office wastepaper fiber biodegradable composites," *Journal of Polymers and the Environment*, vol. 27, no. 6, pp. 1273–1284, 2019.

[46] H. Xiao, W. Lu, and J.-T. Yeh, "Crystallization behavior of fully biodegradable poly(lactic acid)/ poly(butylene adipate-co-terephthalate) blends," *Journal of Applied Polymer Science*, vol. 112, no. 6, pp. 3754–3763, 2009.

[47] S. Jain, M. Misra, A. K. Mohanty, and A. K. Ghosh, "Thermal, mechanical and rheological behavior of poly(lactic acid)/talc composites," *Journal of Polymers and the Environment*, vol. 20, no. 4, pp. 1027–1037, 2012.

[48] Y.-H. Cai, "Crystallization and melting behavior of biodegradable poly(l-lactic acid)/talc composites," *E-Journal of Chemistry*, vol. 9, no. 3, pp. 1569–1574, 2012.

[49] I. R. Mustapa and R. A. Shanks, "Dynamic mechanical properties and melting behaviour of poly(lactic acid)-hemp-nanosilica hybrid composites," in *15th European of conference on composite materials (ECCM15)*, pp. 1–8, Venice, Italy, 2012.

[50] M. S. Alsoufi and A. E. Elsayed, "Surface roughness quality and dimensional accuracy: a comprehensive analysis of 100% infill printed parts fabricated by a personal/desktop cost-effective FDM 3D printer," *Materials Sciences and Applications*, vol. 9, no. 1, pp. 11–40, 2018.

[51] F. R. Ramli, M. S. M. Faudzie, M. A. Nazan et al., "Dimensional accuracy and surface roughness of part features manufactured by open source 3D printer," *APR Journal of Engineering and Applied Sciences*, vol. 13, no. 3, pp. 1139–1144, 2018.

[52] Ultimaker, *Technical and safety data sheets, Ultimaker PLA*, 2018, https://ultimaker.com/en/resources/50461-technical-and-safety-data-sheets.

[53] Polymaker, *Technical data sheet, PolyMax™ PLA*, 2018, https://polymaker.com/product/polymax-PLA.

[54] Polymaker, *Technical data sheet, PolyLite™ PLA*, 2018, https://polymaker.com/product/polylite-PLA.

[55] Polymaker, Technical data sheet, PolyLite™ ABS, *Technical data sheet*, 2018, https://polymaker.com/product/polylite-abs.

[56] 3DXTECH Advanced materials, Tech Data Sheets & Safety Data Sheets, 2018, https://www.3dxtech.com/tech-data-sheets-safety-data-sheets.

[57] BASF - Innofil3D, Technical data sheet PLA by Innofil3D BV, 2017, https://www.ultrafusefff.com/wp-content/uploads/2016/05/TDS-Innofil3D-PLA-160608.pdf.

[58] BASF - Innofil3D, Technical data sheet ABS by Innofil3D BV, 2016, https://www.ultrafusefff.com/wp-content/uploads/2016/05/TDS-Innofil3D-ABS-160609.pdf.